Research Article | Vol. 27, No. 17 | 19 Aug 2019 | OPTICS EXPRESS 24340
Optics EXPRESS

Confocal flowmeter based on self-mixing interferometry for real-time velocity profiling of turbid liquids flowing in microcapillaries

CARLOS YÁÑEZ,* FRANCISCO J. AZCONA, AND SANTIAGO ROYO

Centre for the Development of Sensors, Instruments and Systems, Universitat Politècnica de Catalunya - BarcelonaTech, Rambla Sant Nebridi 10, 08222 Terrassa, Spain
**carlos.rene.yanez@upc.edu*

Abstract: We propose a new confocal device for flow profiling in microcapillaries. A viewfinder system is developed using a visible light microscope, allowing focusing with high precision an 830 nm Fabry-Perot laser diode on a microchannel. By means of a novel confocal approach, the Doppler shift produced by the particles of a turbid liquid moving in the focal plane can be measured in real time using the well-known self-mixing effect. The resolution of this device is characterized in function of the full width at half maximum of the Gaussian frequency peak related to the self-mixing signal in the frequency domain. Velocity measurements for flow rates from 0.2 to 1.6 mL/min are presented, and the results demonstrate that the method reduces the phase noise and the effects of the out-of-focus particles, allowing straightforward flow profiling in microchannel structures.

1. Introduction

The first functional laser was presented in 1960 by Theodore H. Maiman [1]. The invention of this source of monochromatic light is one of the most important scientific breakthroughs in modern history, from engineering to life sciences. In this last area, it has been exploited in applications like laser spectroscopy, microscopy, surgery and as a sensor in non-invasive methods for measuring the velocity of fluids inside the human body [2].

Soon after the laser discovery, the first milestones in laser velocimetry occurred. The first laser Doppler flowmeter (LDF), used for measuring the velocity of a gas flowing inside a glass tube, was reported in 1965 by Forman et. al. [3].

As explained in [4], a conventional LDF estimates the flow velocity by means of the Doppler shift generated in a coherent source of light divided into two optical paths using two different approaches. In the first, an unbalanced scheme is used, a high-intensity beam interacts with the particles of a flow that scatters a small portion of the light over a photodetector (PD) where a low-intensity beam also converges (reference beam mode); and another that uses two beams of equal intensity to generate interference fringes in a focal point, where particles scatter light in any angular direction, then, a PD registers the beating in intensity concerning the Doppler shift (differential Doppler mode).

The basis for an alternative to the double-arm LDF was presented by Rudd [5] in 1968. He investigated the Doppler shift occurring in the light-wave of a He-Ne laser focused onto a rotating mirror, using a PD he registered the modulation of the optical output power (OOP) caused by the small portion of back-reflected light that is re-injected into the laser cavity after interacting with the moving object. Later on, Shinohara et. al. [6] named this phenomenon the *Self-Mixing* effect.

Self-mixing interferometry (SMI), also known as optical feedback interferometry (OFI), is nowadays a well-established technique employed for measuring variables such as absolute distance [7,8], displacement [8,9], vibration and velocity [10]. A SMI-based device is able to perform similar tasks such as a Michelson or Mach–Zehnder interferometer [10], having the additional advantage of being a self-aligned system (an additional reference arm is not

#367274 https://doi.org/10.1364/OE.27.024340
Journal © 2019 Received 10 May 2019; revised 11 Jul 2019; accepted 25 Jul 2019; published 12 Aug 2019

Optics EXPRESS

needed) which in its basic configuration does not require optical components other than a lens for focusing/collimating the laser beam on a target. Additionally, with the emergence of laser diodes (LD) having a monitoring PD integrated in the same packaging, an external PD is not needed anymore.

In recent years, the appearance of biomedical solutions based on SMI has increased [11]. Consequently, SMI flowmeters (SMF), useful for measuring the velocity of biological fluids (both in-vivo and ex-vivo), have been previously reported by other authors [12–15].

In [16] a SMF able to reconstruct the velocity profile of streams with a low particle concentration (single-scattering regime) is presented; however, one of the most critical issues faced by SMF/LDF systems is dealing with turbid media (such as blood flowing into a natural or artificial channel), because of the quantity of particles moving along the channel that causes the photons to interact with more than one particle before to be detected (multiple-scattering regime). Therefore, the Doppler shift registered is not related to the velocity of a single particle, but to the sum of all the scattering events in the light path. This phenomenon is known as phase noise [17], and adds a high degree of uncertainty to the measurement. Additionally, in difference with the double-arm LDF scheme, the sensing volume of a SMF is defined only by the numerical aperture (NA) of the optics that focuses the laser beam on the flow. Thus, all the particles interacting in the focal region, and in a given area close to the near and far field, will contribute to the Doppler spectrum, which causes a significant broadening in the spectrum itself (out-of-focus particles effect) [18].

Several techniques have been presented for overcoming the previous issues [17–22]. Some of them are based on signal processing solutions, which usually make an application in real-time impossible. As an alternative, we propose to provide confocal capabilities to a SMF system, which allows us to exploit the ability of this microscopy technique to instantly define a measurement volume and a sampling depth in the flow profiling of microchannels.

The well-known confocal concept, applied to microscopy, was patented by Minsky [23] in 1961, and the technique revolutionized the field of imaging by allowing researchers to obtain optical information from different depths inside a sample. There is a vast scientific literature on the subject [24–29]. Confocal microscopy is, by its very nature, an imaging technique; the basic idea lies in the use of a spatial filter or pinhole (PH) placed in the conjugated plane to eliminate the out-of-focus light reflected or emitted from the sample under observation. The resolution of a confocal system is related to the full width at half maximum (FWHM) of the intensity point spread function (PSF) produced in the focal plane; in consequence, the resolution is controlled by the numerical aperture of the microscope objective (MO) and the wavelength of the coherent source of light. The diameter of the PH is determined by the balance between sectioning strength (small diameter) and better SNR (large diameter); therefore, the PH size must be optimized for an adequate signal detection, being small enough to reject most of the out-of-focus light without compromising the SNR [25].

Based on the above facts, we define a confocal system as one that uses a mechanical optical filter to reduce the out-of-focus and phase noise effects, which allows unambiguous data acquisition from a very specific focal plane. In the present work, thus, we propose a novel confocal self-mixing (CSMI) approach, where a MO with high-NA (0.55) controls the sensing volume in combination with a spatial filter, reducing the noise produced by the particles moving in the out-of-focus region and the multiple scattered photons that reaches the cavity of an 830 nm Fabry-Perot (FP) laser diode.

It was proposed in [30,31] that a single-mode optical fiber coupled into a laser acts as a spatial filter for achieving confocal performance in microscopy imaging. In [32–34] the SMI signal was obtained by coupling a semiconductor laser onto an optical fiber, and the fiber was later inserted directly into a blood vessel to measure the flow conditions. The Doppler spectrum reported, however, exhibits the typical broadening caused by the phase noise and the out-of-focus particles effect. It is important to note that the authors do not mention any confocal implication in using an optical fiber for SMI sensing.

Optics EXPRESS

In [35] it is stated that the micrometrical cavity of a single-mode laser is equivalent to a PH in confocal microscopy and, therefore, the signal obtained as a result of the modulation of the OOP produced by the back-reflected light that re-enters the cavity is equivalent to a confocal signal. It has been accepted in consequence that SMI is by its very nature a confocal technique. This approach was applied in [36], where a confocal architecture based on the SMI effect is used to image dynamic turbid media by acquiring confocal reflectance and Doppler signals; and in [37], where a confocal laser feedback tomograph based on SMI acquire cross-sectional and volumetric images of a two-layered skin tissue phantom that contains a 200 μm diameter channel where a 10% Intralipid solution flows.

However, we demonstrate that a spatial filter effectively increases the confocal capabilities of a SMI-based flowmeter when is combined with a high-NA microscope objective, which allows real-time velocity profiling in microchannel structures.

This novel confocal device aims to provide the basis towards a medical grade alternative for the diagnosis and prognosis of diseases involving alterations in the characteristics of body fluids moving inside biological or artificial capillaries, in both in-vivo or ex-vivo applications (e.g. determination of the vertical growth phase of cutaneous melanoma, in-vivo burn depth determination, thrombosis, hypercholesterolemia, among others). In addition, we enhance the effectivity of the flow profiling by including a visual tracking system of the laser spot. This allow to focus precisely on a given region of interest, while providing a real-time depth-sectioning capability not presented in other methods.

Next, the theoretical framework is explained; from these bases, the design of our confocal scheme is detailed. In section 3, we characterize the resolution of our system and present the measurements corresponding to the maximum velocity of an emulsion composed by 5% fat milk and 95% distilled water pumped into a microcapillary of ≈235 μm in radius. We compare a non-confocal measurement against three confocal registers for nine different flow rates to demonstrate that our system effectively reduces the phase noise and the out-of-focus particles effect, significantly improving the results. Finally, conclusions are drawn in section 4.

2. Material and methods

2.1. Theoretical approach

Let us considerer a system like the one depicted in Fig. 1, where a laminar fluid under a Newtonian regime flows inside a microcapillary. The velocity profile of this fluid can be described through the Hagen-Poiseuille law:

$$V(r) = V_{\max}\left(1 - \frac{r^2}{R^2}\right). \tag{1}$$

where $V(r)$ is the flow velocity at a given point r from the center of the microcapillary of radius R (where $r = 0$) to its interior wall (where $r = R$). Thus, the maximum velocity V_{max} is found in the center of the channel, tending to become null at the walls.

Optics EXPRESS

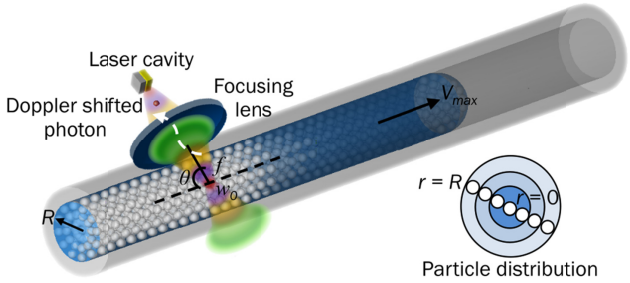

Fig. 1. Schematic diagram of a basic laser Doppler flowmeter based on SMI.

A laser source is focused at the center of the channel, producing a beam waist w_0 at a given focal distance f, where the energy of the radiation reaches its maximum intensity, falling off gradually along the propagation axis in direction to the focusing lens and the far-field. The fluid contains scatterers, which are uniformly distributed in the liquid forming an emulsion; the scatterers flow at a velocity $V(r)$ (dependent on its location r inside the channel), and interact with the photons present in the laser illumination volume, causing a Doppler shift represented by:

$$F_D = \frac{2nV(r)(\cos\theta)}{\lambda}. \tag{2}$$

where F_D is the Doppler-shifted frequency, n is the refractive index of the emulsion, θ is the angle between the laser propagation axis and the velocity vector, and λ is the wavelength of the laser beam in the vacuum.

SMI, equivalently, occurs when a minimal amount of back-scattered photons re-enters the laser cavity through the focusing lens, modulating the OOP of the laser according to the shift in frequency they hold. The modulation in the OOP ($P\tau$) has been explained in [38–40] as:

$$P\tau = P_0[1 + m\mathcal{G}\tau]. \tag{3}$$

$$\mathcal{G}\tau = \cos(\omega_F t). \tag{4}$$

where P_0 is the OOP of the free-running laser without feedback, m is the modulation index of the laser intensity ($\approx 10^{-3}$), $\mathcal{G}\tau$ is the interference function that explains the influence of the feedback in the laser emission, t stands for time and $\omega_F t$ is the light phase under external optical feedback.

The SMI process can be mathematically explained using a Fabry-Perot cavity model, as shown in Fig. 2:

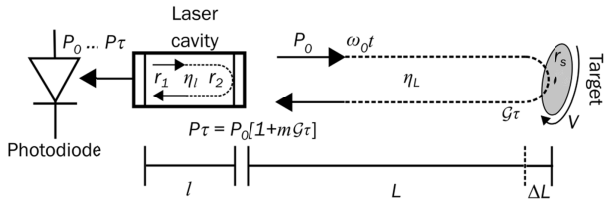

Fig. 2. Scheme of a Fabry-Perot cavity model for a LD under optical feedback.

Where two facets with a reflection coefficient r_1 and r_2 amplifies an injected electromagnetic field until it reaches a lasing threshold state after several round trips inside a cavity of length l (identified as internal cavity). When the resultant emission interacts with the surface of a target moving with a velocity V at a distance L (external cavity), a fraction of the

Optics EXPRESS

light is back-reflected to the laser cavity due to the surface reflection coefficient *rs*. According to [40], the surface roughness must be significant compared to the laser wavelength in order to modulate the external cavity and produce a Doppler shift. This back-reflected field modulates the light phase without feedback $\omega_0 t = 4\pi VLt/\lambda_0$, being λ_0 the laser wavelength without feedback. The light phase under feedback $\omega_F t$ is then found solving the phase equation:

$$\omega_F t = \omega_0 t - C\sin\left(\omega_F t + \arctan\alpha\right). \tag{5}$$

Here, C is the feedback level factor, which is related to the quantity of the back-reflected light that re-enters the cavity, and α is the line-width enhancement factor [41]. C is of special interest because it explains the strength of the changes in the behavior of the laser due to optical feedback; when $C < 1$, a unique solution that satisfies (5) can be found; otherwise, for $C > 1$ several external cavity modes may satisfy the phase equation [42].

C is determined by:

$$C = \gamma\frac{\eta_L}{\eta_l}\sqrt{1+\alpha^2}. \tag{6}$$

where $\eta_L = 2L/c$ and $\eta_l = 2l/c$ are the time of flight in the external and internal cavity respectively, c stands for the speed of light in vacuum, and:

$$\gamma = \frac{r_s}{r_2}\left(1 - r_2^2\right). \tag{7}$$

The time-domain SMI signal obtained due to the modulation in the OOP, exhibits a fringe pattern equivalent to that found in a Michelson or Mach–Zehnder interferometer; therefore, its frequency corresponds to the Doppler frequency associated to the velocity at which the target is moving. This allows a simple frequency analysis by means of an FFT algorithm.

Figure 3 presents experimental results of SMI signals on solid and liquid targets. When the beam interacts with an oscillating solid target, the amplitude of the signal is clear and shows the time dependence of the movement of the target (Fig. 3(a)) and the associated Fourier transform with a single frequency peak (Fig. 3(c)). In the scenario depicted in Fig. 1, where a liquid element is involved, the resulting SMI signal includes the Doppler frequencies corresponding to the velocity *V(r)* of all the photons scattered around the focal point and a certain region above and below it. As a consequence, the time-domain signal becomes much more complex (Fig. 3(b)) and the FFT spectrum obtained will not show a single frequency peak but a broad band of them (Fig. 3(d)).

Optics EXPRESS

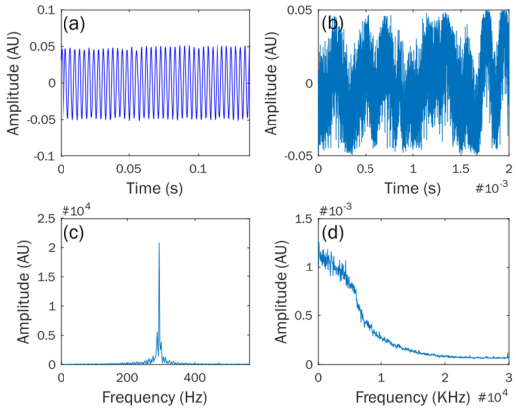

Fig. 3. Comparison between two SMI signals: (a) shows the time-domain signal of an oscillating solid target and (c) its corresponding frequency-domain plot. In (b), the SMI signal was obtained from a turbid liquid flowing inside a pipe. Here, the signal varies in amplitude and frequency according the quantity and velocity of the particles crossing through the illumination volume in a given moment. This is evident in its frequency-domain plot, presented in (d).

2.2. Experimental setup

The proposed confocal flowmeter based on SMI is illustrated in Fig. 4.

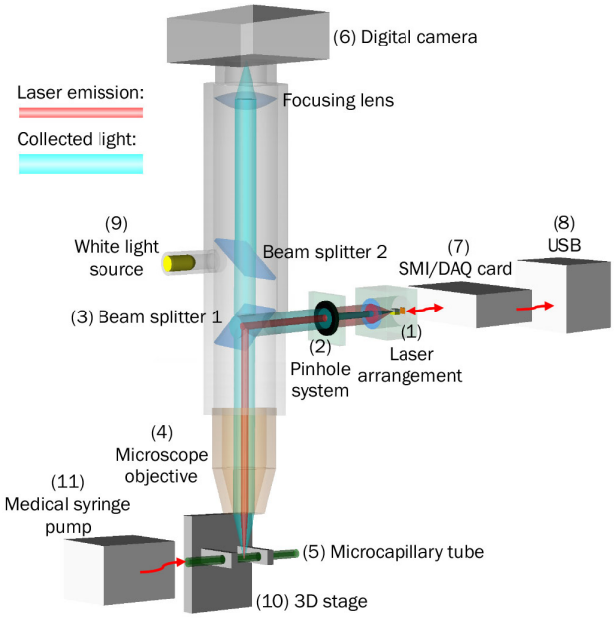

Fig. 4. Schematic diagram of the CSMI flowmeter.

An 830 nm GaAlAs laser diode (Opnext, Inc. HL8338MG) is collimated using a LT220P-B collimation system (Thorlabs, Inc.) (1). An *xy* mechanical stage aligns a pinhole with the center of the laser emission (2), which shapes the beam making it circular and controls the sensing volume. After the pinhole arrangement, the shaped beam arrives to a 50:50 beam splitter (Thorlabs, Inc.) (3), which directs half of the beam towards an infinity-corrected dry microscope objective (4), responsible for focusing the light over a Duran glass microcapillary of ≈235 μm in radius and n = 1.47 (5) and for collecting a portion of the light back-reflected

Optics EXPRESS

from the sample to send it back to the beam splitter. There, half of the reflected light is transmitted to a digital camera (Canon EOS 1000D) (6) which displays a real-time image of the microcapillary and the laser spot. The other optical path passes through the pinhole again, filtering most of the scattered light coming from regions other than the focal plane.

As explained before, the coherent light that makes its way back to the laser cavity after interacting with the scatterers flowing inside the microcapillary, causes a modulation in the LD OOP producing the SMI signal. This phenomenon is registered using the PD included in the LD packaging. The resulting electrical signal is then filtered and amplified by a data acquisition card (7), and processed using a digital oscilloscope with USB communication (Pico Picoscope 4227) (8). Apart from the confocal design, an additional white light source (9) was added for illumination of the sample, a 3-axis mechanical stage (10) is responsible for positioning the microcapillary under the focal plane, and a medical grade syringe pump (Harvard Apparatus Pump 11 Elite) (11) derives an emulsion of 5% fat milk and 95% distilled water into the microcapillary at a controlled flow rate with an accuracy of ± 0.5%.

3. Experiments and results

First, the implications of the pinhole diameter (ø) and the NA of the microscope objective in the sensing volume and SNR are investigated. Six pinholes (Thorlabs, Inc.) with diameters: 1000, 900, 800, 700, 600 and 500 µm (± 10 µm) were tested. They were combined with three different long working distance microscope objectives: 10x, NA = 0.30; 20x, NA = 0.42 and 50x, NA = 0.55 (Optem, LWD, M-Plan Apo).

As it can be seen in Fig. 5, we obtained a well-defined laser spot with each combination and, as expected, the spot size in the focal plane decreases using the highest NA.

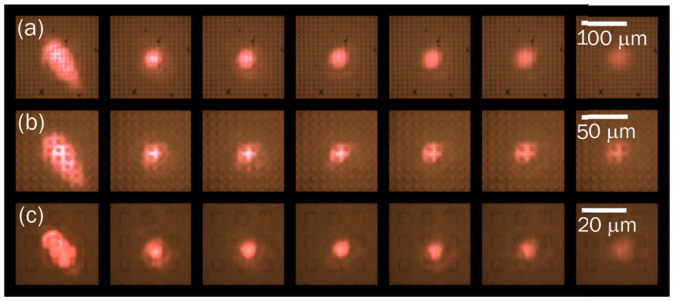

Fig. 5. Laser spots obtained using three different microscope objectives: (a) 10x, NA = 0.3; (b) 20x, NA = 0.42; and (c) 50x, NA = 0.55. Pinhole diameter from left to right: no pinhole, 1000 µm, 900 µm, 800 µm, 700 µm, 600 µm and 500 µm. Scale on the right shows size on the focal plane of the objective.

A smaller PH diameter brings on a better resolution in depth sectioning, but also an expected decay in the optical power, reported in Table 1, which becomes a relevant trade-off of the system. The improvement in the shape of the laser spot due to the PH may be also appreciated in Fig. 5.

Table 1. Optical power measured from each configuration reported in Fig. 4

Microscope objective	Pinhole diameter (µm)						
	No PH	1000	900	800	700	600	500
10x, NA = 0.3	7.21 mW	2.34 mW	1.99 mW	1.69 mW	1.39 mW	1.04 mW	0.78 mW
20x, NA = 0.42	7.22 mW	2.36 mW	1.97 mW	1.72 mW	1.41 mW	1.07 mW	0.78 mW
50x, NA = 0.55	6.17 mW	2.08 mW	1.78 mW	1.52 mW	1.23 mW	0.97 mW	0.68 mW

The OOP measured directly in front of the collimating lens was 22.1 mW. This means that taking into account the losses because of the optical and mechanical elements in the setup,

Optics EXPRESS

when a combination of PH ø = 500 μm and NA = 0.55 MO is used, just ≈3% of the original optical emission reaches the microcapillary. Subsequently, the amount of light power propagated inside the turbid medium that will be back-reflected to the laser cavity and cause the SMI effect will be extremely small. This can be considered both as an advantage and a disadvantage, because in some cases it may be desirable to control the power emission so as not to damage the sample under analysis, especially in biological studies.

The resolution of any confocal system is defined as the ability to discriminate between two different points inside a sample. The greater the resolution, the smaller the minimum distance at which these two points can be recognized as separate objects [43]. As mentioned before, this is related to the NA of the MO and λ. The lack of a reference arm in a SMF configuration implies that the NA will be responsible for the resolution of the system; not only because of the size of the laser spot produced by the optics but for the amount of back-scattered light that will be collected from the diffusive target, influencing therefore the SNR and FWHM of the frequency-domain signal, as reported in [44]. Using a MO of 50x and NA = 0.55, we minimize the elliptical laser spot to $ø_y$ ≈18 μm and $ø_x$ ≈9 μm; and when a PH diameter of 900 μm was employed, the diameter of the spot was reduced up to ≈8 μm. In Fig. 6 we contrast the illumination volume produced by the MO when no PH is used (left) against the volume of a configuration using a PH ø = 900 μm. In agreement with what was explained, the microscope objective of NA = 0.55 was used for the confocal measurements.

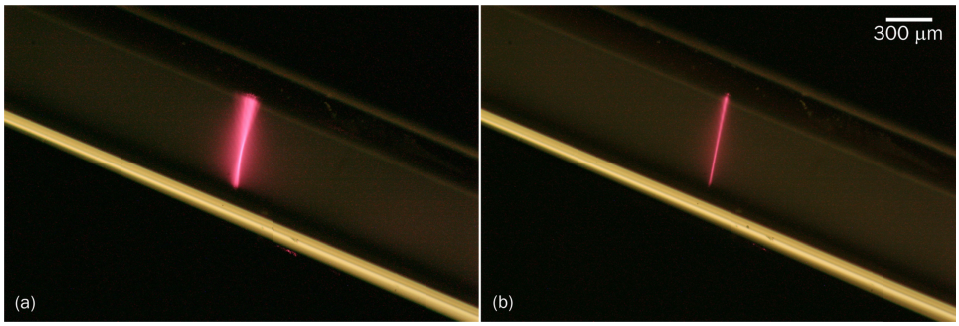

Fig. 6. Comparison between two illumination volumes produced by a 50x microscope objective with NA = 0.55: (a) without pinhole; (b) using a pinhole of 900 μm in diameter. λ = 830 nm.

The viewfinder system, composed by the 50x MO, the white light source and a commercial CMOS camera Canon EOS 1000D, allows to focus the beam precisely at the center of the microcapillary of ≈235 μm in radius. An emulsion composed of 5% fat milk and 95% distilled water was pumped inside the microcapillary at a flow rate of 0.7 mL/min, with the pump rate (PR) controlled by a medical grade syringe pump (Harvard Apparatus Pump 11 Elite) and a 10 mL glass/plastic syringe (Hamilton Gastight 1010 RN) coupled into the microcapillary by means of a neonatal feeding tube (Bet-El).

Using a lateral image of the microcapillary, similar to that shown in Fig. 6, we set the angle between the velocity vector and the beam propagation axis to be θ = 80°. We measured the Doppler shift produced by the particles of fat milk crossing through the focal plane using seven configurations: first, without implying any confocal behavior (without PH); and later, using PH diameters from 1000 to 500 μm.

In Fig. 7, we compare the FWHM of an average of thirty-one frequency spectra obtained from each configuration. As can be interpreted from [40], the low-frequency peaks correspond to the statistical convolution of the effect of the multiple mini-displacements that the particles suffer while crossing the focal plane. Also, other authors describe it as “pedestal” components due to the Gaussian envelope of the Doppler signal [4]. The sharpness of the frequency peaks related to the Doppler shifts occurring in the center of the microcapillary

Optics EXPRESS

suggest that multiple scattering (phase noise) and the out-of-focus particles effect have been reduced [45].

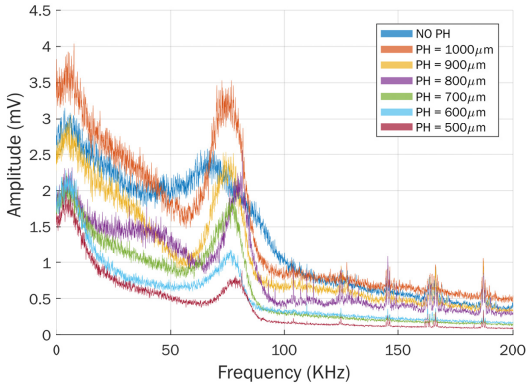

Fig. 7. Comparison between seven frequency spectra obtained from a pumping rate of 0.7 mL/min using seven PH configurations. The FWHM corresponding to a non-confocal measurement (without PH) was 48.86 kHz. For a PH ø from 1000 to 500 µm, the FWHM was 21.12 kHz, 19.85 kHz, 14.93 kHz, 19.68 kHz, 19.17 kHz and 17.64 kHz, respectively.

The FWHM is also related with the scattering coefficient [13] and PR, thus, we used a highly scattering fluid expecting the phase noise to be noticeable in the SMI signal. As the device described here is aimed to provide the basis for a medical device, it is worth noting that fat milk diluted in water is a commonly used phantom that closely resembles the optical properties of blood at 830 nm [11,22,36].

Next, we evaluate several PR using PH ø = 900, 800 and 700 µm. In addition, a non-confocal measurement (without PH) was performed for comparison. In Fig. 8 we present an average of thirty-one measurements for the most significant PR. The maximum PR tested was 1.6 mL/min, whose maximum velocity at the center of the microcapillary theoretically equals to ≈307 mm/s. According to [46], the average blood flow velocity in human vessels varies from 300 mm/s to 0.3 mm/s depending on the vessel type, so we considered that a maximum flow velocity of 300 mm/s would be a good limit for our experiments.

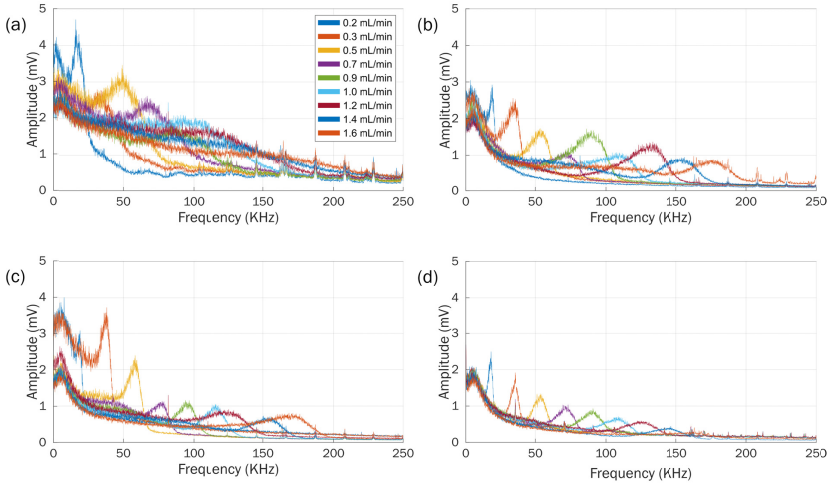

Fig. 8. Frequency spectra for several flow rates (0.2, 0.3, 0.5, 0.7, 0.9, 1, 1.2, 1.4 and 1.6 mL/min): (a) Non-confocal measurement; (b) PH ø = 900; (c) PH ø = 800 and (d) PH ø = 700.

The frequency spectra for the non-confocal measurements are presented in Fig. 8(a). Due to the high-NA microscope objective, it was possible to determine the maximum velocity

Optics EXPRESS

from 0.2 to 0.7 mL/min using the well-known cutoff frequency method [45]; however, from 0.9 to 1.6 mL/min, the Doppler frequency peak cannot be easily determined. In the other hand, in Figs. 8(b)–8(d), the confocal measurements clearly show the frequency peaks related to the Doppler shift that occurs in the center of the microcapillary for all PR. As it can be noticed in Fig. 8(d), the SNR obtained using a PH ø = 700 µm and PR = 1.6 mL/s, was not enough to achieve a confocal measurement. In Fig. 9(a), the theoretical values of the maximum flow velocities and the experimental measurements are contrasted; while in Fig. 9(b) the standard deviation for each flow rate calculated from ninety-three measurements using the three different PH ø (thirty-one for each one) is presented.

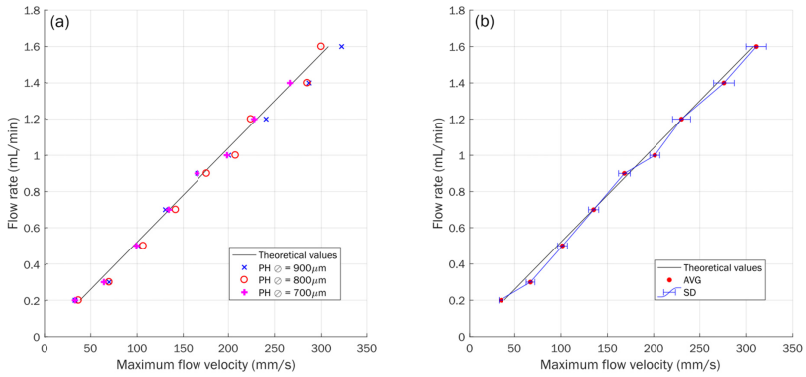

Fig. 9. (a) Plot of the theoretical maximum flow velocities and the experimental results; (b) Standard deviation (SD) obtained for each flow rate based in ninety-three measurements, thirty-one for each PH ø. AVG is the average for each flow rate measurement.

Finally, we used a PH ø = 800 µm to reconstruct the velocity profile of the entire microcapillary for a PR = 0.5 mL/min. First we did a lateral scan, and then a depth sectioning; in both cases, we did thirty-one measurements each 40 µm starting from the center of the microcapillary to the walls. We found that near the microcapillary walls, the frequency peak related to the measured velocity is superimposed on the parasitic low-frequencies of the spectrum, preventing an accurate measurement. Also, the SNR for measurements deeper than ≈995 µm (considering the 36 µm thickness of the microcapillary wall) was too poor to be reliable. This can be attributed either to the effective focal length (EFL) of the MO (4 mm), to the scattering coefficient of the emulsion, or a combination of both. The theoretical Hagen-Poiseuille profile and the confocal measurements are presented in Fig. 10, properly fitting with our measurements.

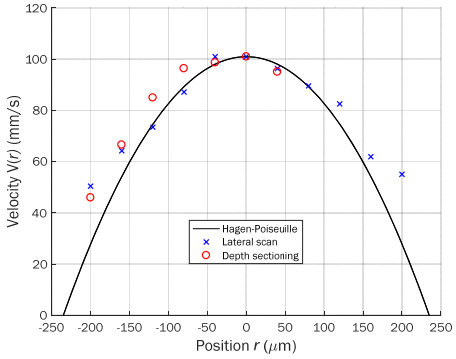

Fig. 10. Plot of the theoretical Hagen-Poiseuille profile and the confocal measurements.

Optics EXPRESS

4. Conclusions

We have presented a prototype of a confocal SMI-based flowmeter, aimed to provide the basis for developing medical resources for the prognosis and diagnosis of diseases involving changes in the velocity profile of body fluids in-vivo and/or ex-vivo, or as auxiliary equipment for infusion therapies. The proposed CSMI system was used to measure the Doppler frequency concerning the maximum velocity present in the center of a laminar flow inside a microcapillary of ≈235 μm in radius in real-time over a highly scattering medium (an emulsion of 5% fat milk and 95% distilled water) and under relatively high flow rates (Up to 1.6 mL/min). Due to our confocal approach, not used in a SMI setup before, no signal processing other than a fast Fourier transform on the signal was needed to obtain the Doppler frequency and the maximum velocity of the particles flowing in the center of the microcapillary. This shows the phase noise and the effect of out-of-focus particles were effectively reduced by using a mechanical optical filter. By integrating an optical microscope in the setup, aiming the laser over a very specific region of interest is possible and allows us to perform non-invasive depth sectioning by changing the focal point along a vertical section of the microcapillary. This feature can be an important tool for the prognosis and treatment of diseases that involve the alteration of the velocity profile of physiological fluids, originated by intrinsic (e.g. embolisms, thrombosis and angiopathies) or extrinsic causes (e.g. traumatisms, burns or iatrogenic effects). Although we have presented an average of thirty-one confocal signals obtained in a single measurement in different conditions, equivalent results can be achieved using a single capture in real time. Yet we have reported here a confocal depth limit of ≈995 μm, this can be improved by varying parameters such as optical output power, pinhole diameter and even the numerical aperture or effective focal length of the microscope objective; this limit also varies depending on the scattering coefficient of the sample under analysis. We are reporting results for a wavelength of 830 nm because at the near-infrared region scattering becomes dominant due to reduced absorption of tissue, usually designated as the diagnostic window. Thus, the SNR in a SMI-based system is improved at this wavelength due to reduced absorption while scattering effects become more visible. However, wavelength can be adapted depending on the optical properties of the target, or the laser safety specifications required on medical applications. Regarding this last issue, the OOP of the laser source and the NA of the MO need be modified in order to meet the laser safety standards according the laser-tissue interactions and the desired application. The results obtained and the requirements of each application should be analyzed individually.

Funding

Consejo Nacional de Ciencia y Tecnología (472102); Ministerio de Economía y Competitividad (FIS2017-89850R).

References

1. T. H. Maiman, “Stimulated optical radiation in ruby,” Nature **187**(4736), 493–494 (1960).
2. H. Jelínková, *Lasers for Medical Applications: Diagnostics, Therapy and Surgery* (Woodhead Publishing, 2013).
3. J. W. Foreman, Jr., E. W. George, and R. D. Lewis, “Measurement of localized flow velocities in gases with a laser Doppler flowmeter,” Appl. Phys. Lett. **7**(4), 77–78 (1965).
4. W. H. Stevenson, “Laser Doppler velocimetry: A status report,” Proc. IEEE **70**(6), 652–658 (1982).
5. M. J. Rudd, “A laser Doppler velocimeter employing the laser as a mixer-oscillator,” J. Phys. Educ. **1**(7), 723–726 (1968).
6. S. Shinohara, A. Mochizuki, H. Yoshida, and M. Sumi, “Laser Doppler velocimeter using the self-mixing effect of a semiconductor laser diode,” Appl. Opt. **25**(9), 1417–1419 (1986).
7. M. Norgia, G. Giuliani, and S. Donati, “Absolute distance measurement with improved accuracy using laser diode self-mixing interferometry in a closed loop,” IEEE Trans. Instrum. Meas. **56**(5), 1894–1900 (2007).
8. Y. L. Lim, K. Bertling, P. Rio, J. R. Tucker, and A. D. Rakic, “Displacement and distance measurement using the change in junction voltage across a laser diode due to the self-mixing effect,” Proc. SPIE **6038**, 60381O (2005).
9. S. Donati, G. Giuliani, and S. Merlo, “Laser diode feedback interferometer for measurement of displacements without ambiguity,” IEEE J. Quantum Electron. **31**(1), 113–119 (1995).

Optics EXPRESS

10. L. Scalise, Y. Yu, G. Giuliani, G. Plantier, and T. Bosch, "Self-mixing laser diode velocimetry: Application to vibration and velocity measurement," IEEE Trans. Instrum. **53**(1), 223–232 (2004).
11. J. Perchoux, A. Quotb, R. Atashkhooei, F. J. Azcona, E. E. Ramírez-Miquet, O. Bernal, A. Jha, A. Luna-Arriaga, C. Yañez, J. Caum, T. Bosch, and S. Royo, "Current developments on optical feedback interferometry as an all-optical sensor for biomedical applications," Sensors (Basel) **16**(5), 694 (2016).
12. F. F. Mul, M. H. Koelink, A. L. Weijers, J. Greve, J. G. Aarnoudse, R. Graaff, and A. C. M. Dassel, "Self-mixing laser-Doppler velocimetry of liquid flow and of blood perfusion in tissue," Appl. Opt. **31**(27), 5844–5851 (1992).
13. M. Norgia, A. Pesatori, and L. Rovati, "Self-mixing laser Doppler spectra of extracorporeal blood flow: A theoretical and experimental study," IEEE Sens. J. **12**(3), 552–557 (2012).
14. S. Cattini, M. Norgia, A. Pesatori, and L. Rovati, "Blood flow measurement in extracorporeal circulation using self-mixing laser diode," Proc. SPIE **7572**, 75720A (2010).
15. J. Herbert, K. Bertling, T. Taimre, A. D. Rakić, and S. Wilson, "Microparticle discrimination using laser feedback interferometry," Opt. Express **26**(20), 25778–25792 (2018).
16. L. Campagnolo, M. Nikolić, J. Perchoux, Y. L. Lim, K. Bertling, K. Loubière, L. Prat, A. D. Rakić, and T. Bosch, "Flow profile measurement in microchannel using the optical feedback interferometry sensing technique," Microfluid. Nanofluidics **14**(1–2), 113–119 (2013).
17. H. Nobach, E. Müller, and C. Tropea, "Efficient estimation of power spectral density from laser Doppler anemometer data," Exp. Fluids **24**, 499–509 (1998).
18. L. Rovati, S. Cattini, and N. Palanisamy, "Measurement of the fluid-velocity profile using a self-mixing superluminescent diode," Meas. Sci. Technol. **22**(2), 025402 (2011).
19. J. B. Roberts and D. B. S. Ajmani, "Spectral analysis of randomly sampled signals using a correlation-based slotting technique," Proc. IEEE **133**(2), 153–162 (1986).
20. R. J. Adrian and C. S. Yao, "Power spectra of fluid velocities measured by laser Doppler velocimetry," Exp. Fluids **5**(1), 17–28 (1986).
21. S. Cattini and L. Rovati, "A simple and robust optical scheme for self-mixing low-coherence flowmeters," Proc. SPIE **8951**, 895102 (2014).
22. M. Nikolić, Y. L. Lim, K. Bertling, T. Taimre, and A. D. Rakić, "Multiple signal classification for self-mixing flowmetry," Appl. Opt. **54**(9), 2193–2198 (2015).
23. M. Minsky, *Microscopy apparatus*, US patent US3013467A (1961).
24. P. M. Conn, *Confocal Microscopy, Volume 307. Methods in Enzymology* (Academic, 1999).
25. J. B. Pawley, *Handbook of Biological Confocal Microscopy* (Springer, 2006).
26. R. F. Guthoff, C. Baudouin, and J. Stave, *Atlas of Confocal Laser Scanning In-vivo Microscopy in Opthalmology: Principles and Applications in Diagnostic and Therapeutic Ophthalmology* (Springer, 2006).
27. B. Matsumoto, *Methods in Cell Biology, Volume 70. Cell Biological Applications of Confocal Microscopy* (Academic, 2002).
28. T. R. Corle and G. S. Kino, *Confocal Scanning Optical Microscopy and Related Imaging Systems* (Academic, 1996).
29. S. W. Paddock, *Methods in Molecular Biology, Volume 122. Confocal Microscopy Methods and Protocols* (Humana, 1999).
30. S. Kimura and T. Wilson, "Confocal scanning optical microscope using single-mode fiber for signal detection," Appl. Opt. **30**(16), 2143–2150 (1991).
31. L. Ginlünas, R. Juškaitis, and S. V. Shatalin, "Scanning fibre-optic microscope," Electron. Lett. **27**(9), 724–726 (1991).
32. M. H. Koelink, F. F. de Mul, A. L. Weijers, J. Greve, R. Graaff, A. C. Dassel, and J. G. Aarnoudse, "Fiber-coupled self-mixing diode-laser Doppler velocimeter: Technical aspects and flow velocity profile disturbances in water and blood flows," Appl. Opt. **33**(24), 5628–5641 (1994).
33. M. Slot, M. H. Koelink, F. G. Scholten, F. F. M. de Mul, A. L. Weijers, J. Greve, R. Graaff, A. C. M. Dassel, J. G. Aarnoudse, and F. H. B. Tuynman, "Blood flow velocity measurements based on the self-mixing effect in a fibre-coupled semiconductor laser: in vivo and in vitro measurements," Med. Biol. Eng. Comput. **30**(4), 441–446 (1992).
34. F. F. M. de Mul, L. Scalise, A. L. Petoukhova, M. van Herwijnen, P. Moes, and W. Steenbergen, "Glass-fiber self-mixing intra-arterial laser Doppler velocimetry: signal stability and feedback analysis," Appl. Opt. **41**(4), 658–667 (2002).
35. R. Juškaitis, T. Wilson, and F. Reinholz, "Spatial filtering by laser detection in confocal microscopy," Opt. Lett. **18**(14), 1135–1137 (1993).
36. A. Mowla, T. Taimre, Y. L. Lim, K. Bertling, S. J. Wilson, T. W. Prow, and A. D. Rakić, "A Compact Laser Imaging System for Concurrent Reflectance Confocal Microscopy and Laser Doppler Flowmetry," IEEE Photonics J. **8**(5), 1–9 (2016).
37. A. Mowla, K. Bertling, S. J. Wilson, and A. D. Rakić, "Dual-Modality Confocal Laser Feedback Tomography for Highly Scattering Medium," IEEE Sens. J. **19**, 6134–6140 (2019).
38. R. Lang and K. Kobayashi, "External optical feedback effects on semiconductor injection laser properties," IEEE J. Quantum Electron. **16**(3), 347–355 (1980).
39. K. Petermann, "External optical feedback phenomena in semiconductor lasers," IEEE J. Sel. Top. Quantum Electron. **1**(2), 480–489 (1995).

Optics EXPRESS

40. T. Taimre, M. Nikolić, K. Bertling, Y. L. Lim, T. Bosch, and A. D. Rakić, "Laser feedback interferometry: a tutorial on the self-mixing effect for coherent sensing," Adv. Opt. Photonics **7**(3), 570–631 (2015).
41. C. H. Henry, "Theory of the linewidth of semiconductor lasers," IEEE J. Quantum Electron. **18**(2), 259–264 (1982).
42. T. Taimre and A. D. Rakić, "On the nature of Acket's characteristic parameter C in semiconductor lasers," Appl. Opt. **53**(5), 1001–1006 (2014).
43. D. W. Piston, "Choosing objective lenses: the importance of numerical aperture and magnification in digital optical microscopy," Biol. Bull. **195**(1), 1–4 (1998).
44. A. Mowla, M. Nikolić, T. Taimre, J. R. Tucker, Y. L. Lim, K. Bertling, and A. D. Rakić, "Effect of the optical system on the Doppler spectrum in laser-feedback interferometry," Appl. Opt. **54**(1), 18–26 (2015).
45. C. Riva, B. Ross, and G. B. Benedek, "Laser Doppler measurements of blood flow in capillary tubes and retinal arteries," Invest. Ophthalmol. **11**(11), 936–944 (1972).
46. I. Fredriksson, M. Larsson, and T. Strömberg, "Optical microcirculatory skin model: assessed by Monte Carlo simulations paired with in vivo laser Doppler flowmetry," J. Biomed. Opt. **13**(1), 014015 (2008).